CHEMISTRY OF MATERIALS

ARTICLE

pubs.acs.org/cm

Diffusion-Driven Formation of MoS_2 Nanotube Bundles Containing MoS_2 Nanopods

Faegheh Hoshyargar, Aswani Yella, Martin Panthöfer, and Wolfgang Tremel*

Institut für Anorganische Chemie und Analytische Chemie, Johannes Gutenberg-Universität, Duesbergweg 10-14, D-55099 Mainz, Germany

Supporting Information

ABSTRACT: MoS_2 nanotube bundles, along with embedded nested fullerenes, were formed in a gas-phase reaction of molybdenum carbonyl and H_2S gas with the assistance of I_2. The amorphous Mo-S-I precursor particles obtained by quenching a modified metal organic chemical vapor deposition (MOCVD) reaction in a large temperature gradient were annealed at elevated temperature in an inert atmosphere. Under the influence of the iodine, the amorphous precursor formed a surface film with an enhanced mobility of the molybdenum and sulfur components. Point defects within the MoS_2 layers, combined with the enhanced surface diffusion, lead to a scrolling of the inherently unstable MoS_2 lamellae. The role of the reaction temperature on the final structure and morphology of the nanotubes, and also the annealing temperature, were studied by X-ray diffraction (XRD) and transmission electron microscopy (TEM). In order to determine the role of iodine as a chemical transport agent, the reaction was carried out in the absence of iodine and with half the amount of iodine. The resulting structures were characterized by scanning electron microscopy (SEM).

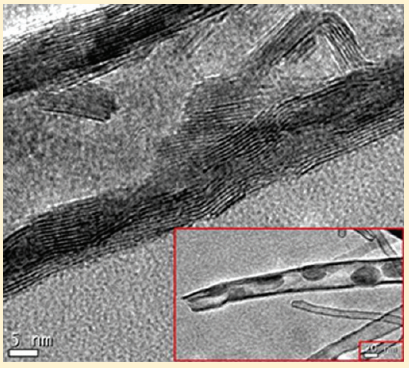

KEYWORDS: chalcogenides, MoS_2 nanotubes, MoS_2 fullerenes, solid state reactivity, MOCVD

INTRODUCTION

The discovery of carbon nanotubes has opened a completely new chapter in the field of novel carbon materials.[1] In analogy with carbon nanotubes, it has been anticipated that other two-dimensional (2D) layered compounds can be "rolled up" to form fullerene-like structures, including tubes, scrolls, and onions.[2] The first inorganic (WS_2) nanotubes were synthesized in 1992.[3] Since that time, a handful of other mesoscopic metal dichalcogenides (TiS_2,[4] SnS_2,[5] VS_2,[6] MoS_2[7]) have been investigated as hollow closed structures of 2D layered materials. In particular, WS_2 and MoS_2 nanoparticles have shown important applications as solid lubricants,[8] photovoltaic film,[9] catalysts,[10] super shock absorbers,[11] etc. Various approaches to other materials forming nanotubes, such as $NiCl_2$,[11] $Ni(OH)_2$,[12] $In(OH)_3$,[13] or V_2O_5[14] have been reported, which implies that, generally, substances crystallizing in layered structures may form nanotubes under favorable conditions.

Tenne et al.[15] were the first to report the production of macroscopic quantities of fullerene-like MoS_2 nanotubes via the gas-phase reaction between MoO_{3-x} and H_2S in a reducing atmosphere at elevated temperatures (800−950 °C). Subsequently, the reaction mechanisms associated with particle formation were studied extensively.[16] Dorhout et al.[7a] used relatively low temperatures (~400 °C) for annealing ammonium thiomolybdate within an alumina template. MoS_2 nanotubes with poor crystallinity were obtained, while the high-temperature approach (~1300 °C) of Rao's group[7c] led to the formation of well-ordered tubes, but only in very low yields. Remskar and co-workers obtained MoS_2 nanotubes by chemical transport.[7d] Ghosh et al. showed the synthesis of honeycomb-like MoS_x nanoporous/mesoporous layer structures via the electrochemical deposition of MoS_x nanoplates from aqueous solutions on NiP and CoW substrates and subsequent annealing.[7e]

Numerous new types of nanotubes and nanoparticles have been synthesized in recent years. Among them, the synthesis of core−shell nanotubes, such as PbI_2@WS_2,[17] the so-called "MoS_2 mama-tubes",[18] and others have been described. The synthesis of macroscopic amounts of INT-WS_2, using a fluidized-bed reactor, has been reported recently.[19] According to atomic force microscopy (AFM) investigations assisted by density functional-based tight binding (DFTB) calculations, individual WS_2 nanotubes exhibit a Young modulus of ~150−170 GPa and a tensile strength of 16 GPa.[20]

The synthetic challenge in the synthesis of MoS_2 hollow nanoparticles such as nanotubes and nested fullerenes is that they are high-temperature and low-pressure phases that are not accessible via traditional solid-state routes. In conventional high-temperature reactions, the energy required for the solid-state diffusion of the reactants would exceed the nucleation energy of the metastable MoS_2 nanoparticles. A consequence of these bulk reactions is that only the thermodynamically stable final phase (i.e., 2H-MoS_2) is obtained. In contrast, reactions in which solid-state diffusion plays only a minor role are kinetically controlled.[21]

Received: May 24, 2011
Revised: September 4, 2011
Published: October 05, 2011

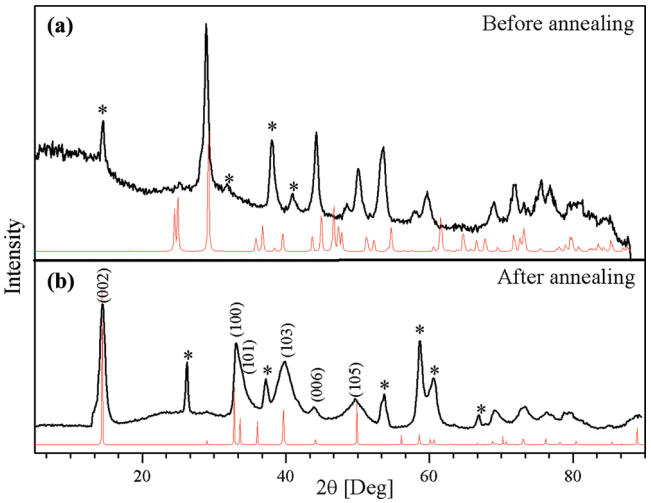

Figure 1. (a) Powder X-ray diffraction (XRD) pattern of the primary product obtained from the reaction of $Mo(CO)_6$, I_2, and H_2S/Ar at 550 °C; the red trace line indicates I_2 (PDF-2 File Card No. 43-0304). (b) Powder XRD pattern of the primary product after annealing at 850 °C; the red line corresponds to 2H-MoS_2 (PDF-2 File Card No. 37-1492), and the asterisks indicate reflections from $Mo_2S_5I_3$ (PDF-2 File Card No. 39-0717).

Therefore, a metastable phase may nucleate and grow until its growth exhausts the supply of the reactants. The sequence of phases formed is dependent upon the relative activation energies for the nucleation of various compounds, and compounds in the equilibrium phase diagram may be temporarily skipped if they have a large activation energy for nucleation. In fact, all synthetic approaches to hollow chalcogenide nanoparticles rely on circumventing the solid-state diffusion step.[22]

Our approach to bypass solid-state diffusion as a rate-determining step is based on a gas-phase reaction. In some recent contributions, the gas-phase synthesis of MS_2 (M = Sn, Mo, W, Re) nested particles was reported with the aid of a metallorganic chemical vapor deposition (MOCVD)-based reaction.[23] In a first step, amorphous chalcogenide nanoparticles were formed in a gas-phase reaction from the precursors $Mo(CO)_6$ and sulfur or selenium, respectively. Annealing of these amorphous nanoparticles at moderate temperature leads to the formation of nested fullerene species. Attempts to enhance the atom mobility through surface diffusion by adding iodine as a mineralizing agent in this MOCVD reaction lead to the formation of partially amorphous primary structures with micrometer-scale dimensions. Upon annealing of these primary Mo/S/I particles, radially oriented arrays of hollow nanotubes containing nested structures in a peapod-like fashion were formed.

EXPERIMENTAL METHODS

Synthesis of MoS_2 Nanotubes. The reaction was carried out in a three-zone horizontal tube furnace. Five hundred milligrams (500 mg) of $Mo(CO)_6$ were weighed inside the glovebox and was transferred outside the box in a corundum boat in an argon-filled chamber. Typically, 1000 mg of iodine was weighed and mixed with molybdenum carbonyl immediately before starting the reaction. Prior to the synthesis, the setup was flushed with argon for at least 30 min. Subsequently, the corundum boat was placed into a glass tube with an inner diameter of 15 mm, and the glass tube was placed in the upstream end of an reaction tube of an outer diameter of 35 mm inside a three-zone horizontal furnace. Argon was flushed through this setup for another half hour. The three zones were then heated to 550 °C at a rate of 10 °C/min. When the temperature reached to 550 °C, the boat was moved to the center of the furnace and the setup was flushed with H_2S for 1 h. After the heating step, the temperature was decreased to room temperature with the rate of 10 °C/min under argon and the product was collected with a spatula from the outer wall of the small and the inner wall of the bigger glass tubes.

Thermal Annealing. The collected material was subjected to thermal annealing in a conventional tube furnace. The annealing was performed by transferring the sample from the first step into a corundum boat and placing it in the middle of a horizontal tube furnace at a temperature of 850 °C with a heating rate of 5 °C/min under constant argon gas flow of 100 sccm for 1 h. To see how the annealing temperature affects the composition and the morphology of final product, annealing was performed at temperatures of 750°, 800°, and 900 °C as well, and the products were used for further characterizations.

Material Characterization. X-ray diffraction (XRD) patterns were recorded using a Siemens Model D5000 diffractometer that was equipped with a Braun Model M50 position-sensitive detector in transmission mode using Ge (200) monochromatized Cu Kα radiation. Samples were prepared between two layers of cellophane tape. Crystalline phases were identified according to the PDF-2 database, using Bruker AXS EVA 10.0 software.

The product was characterized using high-resolution scanning electron microscopy (HRSEM) (LEO Model 1530 field-emission scanning electron microscopy (SEM) system, 6 kV extraction voltage). Transmission electron microscopy (TEM) was carried out on a Philips Model EM420 instrument with a twin lens and a Philips Model CM12 instrument with a twin lens at an acceleration voltage of 120 kV. High-resolution images were taken with a Philips Model FEI TECNAI F30 ST electron microscopy system (field-emission gun, 300 kV extraction voltage) that was equipped with an Oxford EDX (energy-dispersive X-ray) spectrometer with a Si/Li detector and an ultrathin window for elemental analysis. Samples for TEM studies were prepared from ethanolic suspensions of the samples. Three drops of the sonicated suspension were administered onto a copper grid that was coated with an amorphous carbon layer.

RESULTS AND DISCUSSION

The powder XRD patterns of the product obtained after the first step and after annealing are shown in Figure 1a. The diffraction pattern of the primary product could be assigned to I_2 (PDF-2 File Card No. 43-0304) and 2H-MoS_2 (PDF-2 File Card No. 37-1492). The product obtained after annealing showed a high degree of crystallinity, and most of the reflections could be assigned to 2H-MoS_2 and an impurity of $Mo_2S_5I_3$ (PDF-2 File Card No. 39-0717). This impurity phase is marked with an asterisk in Figure 1b.

The primary product obtained after the first reaction step was characterized using SEM and TEM. The SEM image in Figure 2a shows that the product obtained at 550 °C consisted mainly of microspheres with diameters of ~1−2 μm and some 2D flat nanostructures with a common origin and branches with a typical length of 5−8 μm (marked with a red square in Figure 2a). The magnified SEM image of the microspheres (Figure 2b) also shows branches emanating from a common origin. The high-resolution

dx.doi.org/10.1021/cm201460z |Chem. Mater. 2011, 23, 4716–4720

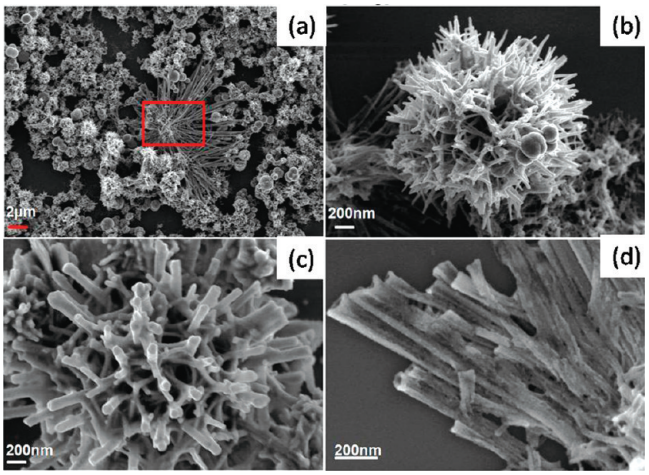

Figure 2. SEM images of the product obtained after the first step. (a) Overview SEM image of the product. The 2D branched nanostructures are marked by a red rectangle. (b) Magnified image of the microspheres showing branched MoS_2 nanowires emanating from the center. (c) High-resolution (HR) image showing the branched nanowires in a top view. (d) HR image of the branched 2D nanostructures with open-ended tips and porous walls.

(HR) image in Figure 2c reveals the individual MoS_2 branches to have average diameters of ~50 nm. The branch substructures of the microspheres were found to be solid with a smooth surface, whereas the branches of the 2D flat nanostructures were consistently open-ended (Figure 2d) with porous walls.

The product was further characterized by a combined TEM/EDX analysis. Figure S1a in the Supporting Information shows a typical TEM image of one individual MoS_2 microsphere nanostructure, which indicates that the MoS_2 nanotubes emanating from the center are straight with relatively uniform diameters over their entire length (average length of ~400 nm). The tubular morphology of the MoS_2 nanostructure is clearly visible at the open ends. The sample released iodine under high vacuum conditions in the TEM system, which presumably results in the formation of an open-ended tube structure under in situ conditions. The particles attached to the outer walls of the tubes were formed under high vacuum, probably because of the release of iodine. The branched microsphere-type structures were stable even after long periods of ultrasonic treatment. This indicates their robustness, while the 2D branched nanostructures were less stable upon sonication, as shown in Figure S1b in the Supporting Information. HRTEM analysis shows that the product was completely amorphous.

Annealing of the product was carried out at 850 °C under argon, and, after annealing, a highly crystalline product was obtained. Most of the reflections in the powder pattern could be assigned readily to 2H-MoS_2. The reflections marked with an asterisk could be assigned to $Mo_2S_5I_3$.[24]

Figure 3 shows TEM and HRTEM images of the product obtained after annealing. The SEM images (see Figure S2 in the Supporting Information) resemble those of the product before annealing. However, the TEM images clearly show that, after annealing, the tubular 1D nanowires emanating from the microspheres became crystalline and transformed to nanotubes. Most tips of the tubes were closed, and some of the tubes were filled with some particles (in the middle of the tube) bearing resemblance to a "peapod-like" structure, as shown in Figure 3b.

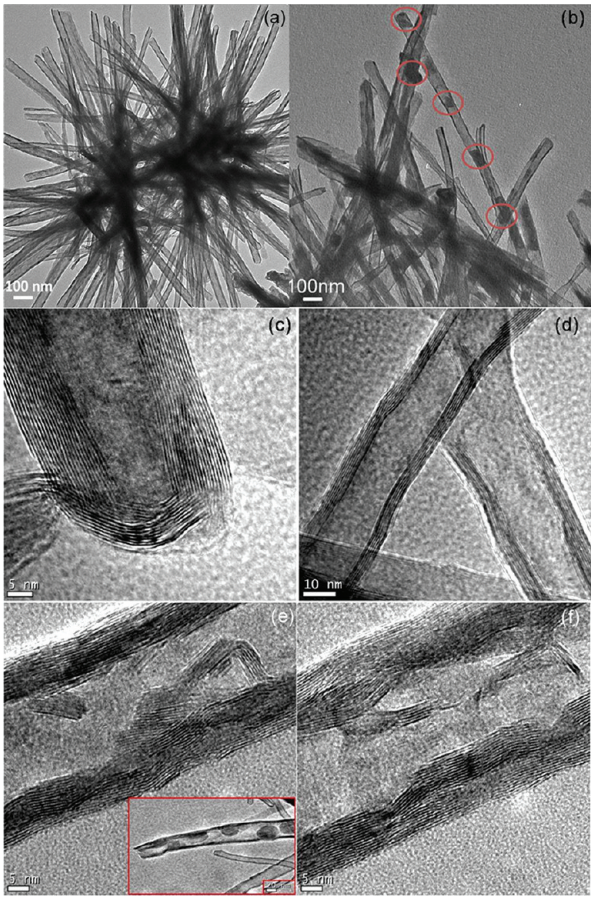

Figure 3. TEM images of the product obtained after annealing ((a) TEM image of a single microsphere, showing the nanotubes emanating from the center an a radial manner; (b) TEM image showing the ends of the microsphere with a peapod-like structure). HRTEM images of the product obtained after annealing ((c) closed-end nanotube, (d) open-ended nanotube, (e) peapod-like structure with nested fullerenes inside the nanotubes, and (f) a "burst" fullerene under the beam).

The HRTEM image in Figure 3c shows the closed tip of a MoS_2 nanotube. The interlayer spacing of 0.63 nm between the layers in the nanotubes is slightly larger than the (002) *d*-spacing of 2H-MoS_2. The "peapod-like" nanotubes were found to be quite unstable under the intense electron beam, and the fullerene-like particles (see Figures 3e and 3f) inside were found to open up under the beam to form bent aggregates of sheets. In order to investigate how the annealing temperature affects the structure and morphology of MoS_2 nanotubes, thermal annealing of the product was carried out at 750, 800, and 900 °C. Annealing at lower temperature of 750 °C in argon resulted in the formation of tubes with more defects, as seen from the TEM and HRTEM image in Figure S3 in the Supporting Information. At 800 °C, the formation of the "peapod-like" nanotubes is observed, as shown in Figure S4 in the Supporting Information, and the nanotubes have still defects, in comparison to those obtained at 850 °C. Annealing at an elevated temperature (900 °C) resulted in complete collapse of the nanotubes (see Figure S5 in the Supporting Information) and an elemental molybdenum residue was observed, according to phase analysis from powder XRD. The reaction was also performed at lower temperatures (i.e., 350 and 450 °C) and the product obtained was annealed at 850 °C under

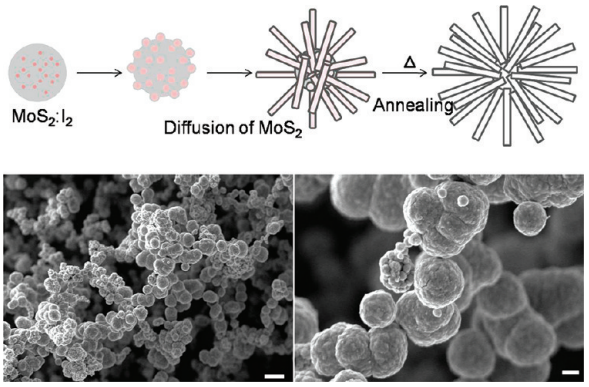

Figure 4. (Top) Scheme illustrating the growth of MoS_2 nanotube bundles in the presence of iodine. (Bottom) SEM images of the product obtained without using iodine in the process ((a) overview SEM image showing that the product consists of spherical particles; (b) magnified image showing that the surface is not uniform but rather consists of smaller aggregates).

an argon atmosphere. The TEM images of the product obtained at 350 °C are shown in Figure S6 in the Supporting Information. The "cookie-like" structures seem to be spherical analogues of the "peapod-like" nanotubes. At 450 °C, the branches of the nanotube bundles are about to emerge (see Figure S7 in the Supporting Information). EDX analysis of the product obtained after annealing showed the presence of MoS_2, along with a small amount of iodine, which is consistent with the powder diffraction pattern.

In order to determine the role of iodine, the reaction was carried out in the absence of iodine, using only $Mo(CO)_6$ and H_2S as precursors. The SEM images of the product obtained in the absence of iodine are shown in Figure 4. The product now contained exclusively spherical particles that, in turn, were aggregates of smaller particles. Hence, the formation of the microspheres might be caused by the thermal decomposition of the amorphous Mo-S-I precursor, which leads to an outward diffusion flow of iodine (as indicated by the second arrow in the scheme shown in Figure 4) via the formation of hollow tubes upon annealing.

The fact that the MoS_2 nanotubes grow from a common nucleation point indicates that a MoS_2 "cluster" might occur in the course of the growth process. For the reorganization of the MoS_2 structure and the formation of MoS_2 nanotubes, defect annealing processes seems to play a prominent role. This defect annealing can only proceed smoothly when surface diffusion is rapid enough,[25] i.e., at elevated temperatures ($T \approx 850$ °C). In accordance with this interpretation, powder XRD and electron microscopy showed that MoS_2 nanostructures obtained in the presence of iodine are well-crystallized and well-ordered (2H-MoS_2), while those obtained in the absence of iodine do not form hollow structures and display a significantly higher defect density, as seen from the TEM image in Figure S8 in the Supporting Information. The use of smaller amounts of iodine decreased the crystallinity of the products (see the SEM image shown in Figure S9 in the Supporting Information for half the amount of iodine), which indicates that ordering by surface diffusion is caused mainly by iodine.

The proposed growth mechanism may be contrasted with the vapor−liquid−solid (VLS) growth mechanism for nanorods or nanotubes. In this metal-catalyzed nanorods/tube synthesis, almost monodisperse metal nanoclusters can be used to control the diameter[5,26] and (through growth time) the length[27] of Group III−V and Group IV semiconductor nanowires.[28] The vapor-phase reactants required for nanorods/tube growth are supplied by an inert carrier gas that provides the required dilution of the reactive vapor-phase species. The metal droplets catalyze the formation of nanorods/tubes by providing a nucleation surface. In principle, this approach can be successfully implemented if a proper catalyst suitable for the growth of the metal chalcogenide can be identified.[5] It is apparent that the nanotubes reported in this work clearly grow via a different mechanism. The chalcogenide nanotubes grow from a "catalytic" metal droplet in an outward direction, and the catalyst remained fixed at the end of the tube.

CONCLUSIONS

In conclusion, we have synthesized MoS_2 nanotube bundles emanating from a common origin in a radial manner. The iodine content of the precursors leads to the formation of a surface film that makes the molybdenum and sulfur atoms mobile, via isothermal chemical transport. The enhanced mobility of the Mo and S constituents aids in the formation of point defects within the MoS_2 layers that are needed to scroll up the inherently instable MoS_2 sheets. In the resulting tubular structures, the number of dangling bonds and, therefore, the total surface energy are decreased. The diffusion flow of the volatile reaction intermediates from the inside of the precursor particles to the outside of the precursor particles leads to the formation of nanotube bundles containing "peapod-like" MoS_2, which are mechanically stable upon sonication. The extension of this new synthesis approach to other layer-structure metal sulfides is subject of ongoing investigations.

ASSOCIATED CONTENT

Supporting Information. TEM images of the product obtained after the first step (Figure S1); SEM images of the product obtained after the annealing (Figure S2); TEM overview and HRTEM images of the product obtained at the annealing temperature of 750 °C (Figure S3); TEM image of the product obtained at the annealing temperature of 800 °C (Figure S4); TEM image of the product obtained at the annealing temperature of 900 °C (Figure S5); TEM image of the product obtained at the reaction temperature of 350 °C (Figure S6); TEM image of the product obtained at the reaction temperature of 450 °C (Figure S7); TEM image of the product obtained after omitting iodine as precursor (Figure S8); SEM image of the product obtained using half the amount of iodine (Figure S9). This information is available free of charge via the Internet at http://pubs.acs.org/.

AUTHOR INFORMATION

Corresponding Author

*Tel.: +49 6131 39 25135. Fax: +49 6131 39 25605. E-mail: tremel@uni-mainz.de.

ACKNOWLEDGMENT

This work was supported by the Deutsche Forschungsgemeinschaft (DFG) within the priority program 1165 "Functionalization of Inorganic Chalcogenide Nanotubes: From Controlled Synthesis to Organized Assembly and Function". F.H. is a recipient of an IMPRS fellowship from MAINZ, the Graduate School of Excellence of the State of Rhineland−Palatinate. We acknowledge

support for the Electron Microscopy Center in Mainz (EZMZ) from the Center for Complex Matter (COMATT).

REFERENCES

(1) (a) Iijima, S. *Nature* **1991**, *354*, 56–58.(b) Dresselhaus, M. S.; Dresselhaus, G.; Eklund, P. C. *Science of Fullerenes and Carbon Nanotubes.*: Academic Press: New York, 1996.

(2) (a) Tremel, W. *Angew. Chem.* **1999**, *111*, 2311–2315. *Angew. Chem., Int. Ed.* **1999**, *38*, 2175–2179. (b) Patzke, G.; Krumeich, F.; Nesper, R. *Angew. Chem.* **2002**, *114*, 2554–2571. *Angew. Chem., Int. Ed.* **2002**, *41*, 2446–2461.

(3) Tenne, R.; Margulis, L.; Genut, M.; Hodes, G. *Nature* **1992**, *360*, 444–446.

(4) Chen, J.; Li, S.-L.; Tao, Z.-L.; Shen, Y.-T.; Cui, C.-X. *J. Am. Chem. Soc.* **2003**, *125*, 5284–5285.

(5) Yella, A.; Mugnaioli, E.; Panthöfer, M.; Therese, H. A.; Kolb, U.; Tremel, W. *Angew. Chem.* **2009**, *121*, 6546–6551. *Angew. Chem., Int. Ed.* **2009**, *48*, 6426–6430.

(6) Therese, H. A.; Rocker, F.; Reiber, A.; Li, J.; Stepputat, M.; Glasser, G.; Kolb, U.; Tremel, W. *Angew. Chem.* **2005**, *117*, 267–270. *Angew. Chem., Int. Ed.* **2005**, *44*, 262–265.

(7) (a) Zelenski, C. M.; Dorhout, P. *J. Am. Chem. Soc.* **1998**, *120*, 734–742. (b) Chen, J.; Kuriyama, N.; Yuan, H.; Takeshita, H. T.; Sakai, T. *J. Am. Chem. Soc.* **2001**, *123*, 11813–11814. (c) Nath, M.; Govindaraj, A.; Rao, C. N. R. *Adv. Mater.* **2001**, *13*, 283–286. (d) Remškar, M.; Mrzel, A.; Viršek, M.; Jesih, A. *Adv. Mater.* **2007**, *19*, 4276–4278. (e) Ghosh, S. K.; Bera, T.; Karacasa, O.; Swarnakar, A.; Buijnsters, J. G.; Celis, J. P. *Electrochim. Acta* **2011**, *56*, 2433–2442.

(8) (a) Rapoport, L.; Bilik, Y.; Feldman, Y.; Homyonfer, M.; Cohen, S. R.; Tenne, R. *Nature* **1997**, *387*, 791. (b) Rapoport, L.; Leshchinsky, V.; Volovik, Y.; Lvovsky, M.; Nepomnyashchy, O.; Feldman, Y.; Popovitz-Biro, R.; Tenne, R. *Surf. Coat. Technol.* **2003**, *163−164*, 405–412.

(9) Homyonfer, M.; Alperson, B.; Rosenberg, Y.; Sapir, L.; Cohen, S. R.; Hodes, G.; Tenne, R. *J. Am. Chem. Soc.* **1997**, *119*, 2693–2698.

(10) (a) Iwata, Y.; Sato, K.; Yoneda, T.; Miki, Y.; Sugimoto, Y.; Nishyima, A.; Shimada, H. *Catal. Today* **1998**, *45*, 353–359. (b) Lauritsen, J. V.; Kibsgaard, J.; Helveg, S.; Topsøe, H.; Clausen, B. S.; Lægsgaard, E.; Besenbacher, F. *Nat. Nanotechnol.* **2007**, *2*, 53–58.

(11) Hachohen, Y. R.; Grunbaum, E.; Sloan, J.; Hutchison, J. L.; Tenne, R. *Nature* **1998**, *395*, 336–337.

(12) Cai, F.-S.; Zhang, G.-Y.; Chen, J.; Gou, X.-L.; Liu, H.-K.; Dou, S.-X. *Angew. Chem.* **2004**, *116*, 4308–4312. *Angew. Chem., Int. Ed.* **2004**, *43*, 4212–4216.

(13) Fang, Y.; Wen, X.; Yang, S. *Angew. Chem.* **2006**, *118*, 4771–4774. *Angew. Chem., Int. Ed.* **2006**, *45*, 4655–4658.

(14) Spahr, M. E.; Bitterli, P.; Nesper, R. *Angew. Chem.* **1998**, *110*, 1339–1342. *Angew. Chem., Int. Ed.* **1998**, *37*, 1263–1265.

(15) (a) Hershfinkel, M.; Gheber, L. A.; Volterra, V. A.; Hutchison, J. L.; Tenne, R. *J. Am. Chem. Soc.* **1994**, *116*, 1914–1917. (b) Feldman, Y.; Wasserman, E.; Srolovitz, D. J.; Tenne, R. *Science* **1995**, *267*, 222–225.

(16) Rothschild, A.; Sloan, J.; Tenne, R. *J. Am. Chem. Soc.* **2000**, *122*, 5169–5179.

(17) Kreizman, R.; Hong, S.-Y.; Sloan, J.; Popovitz-Biro, R.; Albu-Yaron, A.; Tobias, G.; Ballesteros, B.; Davis, B. G.; Green, M. L. H.; Tenne, R. *Angew. Chem.* **2009**, *121*, 1256–1259. *Angew. Chem., Int. Ed.* **2009**, *48*, 1230–1233.

(18) Remskar, M.; Mrzel, A.; Virsek, M.; Jesih, A. *Adv. Mater.* **2007**, *19*, 4276–4279.

(19) Zak, A.; Sallacan-Ecker, L.; Margolin, A.; Genut, M.; Tenne, R. *Nano* **2009**, *4*, 91–98.

(20) (a) Kaplan-Ashiri, I.; Cohen, S. R.; Gartsman, K.; Rosentsveig, R.; Seifert, G.; Tenne, R. *J. Mater. Res.* **2004**, *19*, 454–459. (b) Kaplan-Ashiri, I.; Tenne, R. *J. Cluster Sci.* **2007**, *18*, 549–563.

(21) (a) Schneidmiller, R.; Bentley, A.; Hornbostel, M. D.; Johnson, D. C. *J. Am. Chem. Soc.* **1999**, *121*, 3142–3149. (b) Noh, M.; Johnson, D. C. *J. Am. Chem. Soc.* **1996**, *118*, 9117–9122. (c) Harris, F. R.; Standridge, S.; Feik, C.; Johnson, D. C. *Angew. Chem.* **2003**, *115*, 5454–5457. *Angew. Chem., Int. Ed.* **2003**, *42*, 5296–5299.

(22) (a) Hong, S. Y.; Popovitz-Biro, R.; Prior, Y.; Tenne, R. *J. Am. Chem. Soc.* **2003**, *125*, 10470–10474. (b) Gordon, J. M.; Katz, E. A.; Feuermann, D.; Albu-Yaron, A.; Levy, M.; Tenne, R. *J. Mater. Chem.* **2008**, *18*, 458–462. (c) Parilla, P. A.; Dillon, A. C.; Parkinson, B. A.; Jones, K. M.; Alleman, J.; Riker, G.; Ginley, D. S.; Heben, M. J. *J. Phys. Chem. B* **2004**, *108*, 6197–6207.

(23) (a) Etzkorn, J.; Therese, H. A.; Rocker, F.; Zink, N.; Kolb, U.; Tremel, W. *Adv. Mater.* **2005**, *17*, 2372–2375. (b) Zink, N.; Pansiot, J.; Kieffer, J.; Therese, H. A.; Panthöfer, M.; Rocker, F.; Kolb, U.; Tremel, W. *Chem. Mater.* **2007**, *19*, 6391–6400. (c) Yella, A.; Therese, H. A.; Zink, N.; Panthöfer, M.; Tremel, W. *Chem. Mater.* **2008**, *20*, 3587–3593. (d) Yella, A.; Mugniaoli, E.; Therese, H. A.; Panthöfer, M.; Tremel, W. *Chem. Mater.* **2009**, *21*, 2474–2481.

(24) Perrin, C.; Perrin, A.; Prigent, J. *Bull. Soc. Chim. Fr.* **1972**, *8*, 3086–3091.

(25) Schäfer, H. *Angew. Chem.* **1971**, *83*, 35–42.

(26) Gudiksen, M. S.; Lieber, C. M. *J. Am. Chem. Soc.* **2000**, *122*, 8801–8802.

(27) Cui, Y.; Lauhon, L. J.; Gudiksen, M. S.; Wang, J. F.; Lieber, C. M. *Appl. Phys. Lett.* **2001**, *78*, 2214–2216.

(28) Wagner, R. S. In *Whisker Technology*; Wiley−Interscience: New York, 1970; pp 47−119.